#1

Geochimica et Cosmochimica Acta, 1963, Vol. 27, pp. 623 to 637. Pergamon Press Ltd. Printed in Northern Ireland

Electron microanalysis of metallic meteorites
Part 1—Phosphides and sulfides

JOSEPH I. GOLDSTEIN and ROBERT E. OGILVIE*

(*Received* 8 *August* 1962; *in revised form* 26 *November* 1962)

Abstract—The composition of phosphide and sulphide precipitates in the Canyon Diablo, Breece and Grant meteorites were examined with the electron microanalyzer. The phosphides had a composition of 15·5 wt% P, between 20 and 46 wt% Ni, 0·1 wt% Co with Fe as the remaining constituent. The sulfide precipitates had a composition of stoichiometric FeS with no solubility for Ni. The regions of swathing kamacite around the phosphide particles had a Ni depletion of from 0·5 to 2 wt%.

Excluding the massive phosphides, which are unrelated to the kamacite structure, it is concluded that the schreibersite nucleated within the supersaturated kamacite in the temperature range from 700 to 500°C while rhabdite formed between 500 and 400°C. The variation in the composition of the phosphides is due to the limited diffusion of Ni from kamacite to the phosphide at lower temperatures.

The very large troilite particles are formed directly from the molten state. However, sulfides also precipitate from the solid state below the eutectic temperature and grow with the rejection of both iron and nickel into the region surrounding the particle, called swathing kamacite.

I. INTRODUCTION

METEORIC structures have fascinated investigators since the early 1800's and a large number of studies have been conducted to determine their composition, structure, and the thermal history by which they formed. The purpose of this study was to determine the composition of meteoric phosphides and sulfides and from such data, to establish the method by which these structures might have formed.

The determination of the chemical composition of these minerals has unfortunately been hampered to date because the chemical techniques used required a relatively large amount of material for analysis. With the advent of the electron microanalyzer, it is now possible to determine with a high degree of accuracy not only the average particle composition but also compositional variations within the individual particles.

It has been demonstrated (CASTAING, 1952) that the electron microanalyzer can measure the composition of an extremely small volume of material. Essentially the technique employs an electron optical system that focuses an electron beam on the surface of the specimen to be examined. The size of the irradiated area is of the order of 1 μ in diameter. The depth of penetration of the electrons is of the same order of magnitude so that the X-ray spectrum which results originates from a few millionths of a microgram of material. The subsequent analysis of the X-ray spectrum allows one to determine the chemical composition for elements in the periodic table from sodium through uranium.

Since the introduction of this instrument, several studies have been published

*Department of Metallurgy, Massachusetts Institute of Technology, Cambridge, Massachusetts.

on the compositions of the metallic phases in meteorites (WITTRY, 1957; YAVNEL *et al.* 1958; MARINGER *et al.* 1959; FELLER-KNIEPMEYER and UHLIG, 1961). However, only a very limited amount of work has been published on the composition of metallic phosphides (ADLER and DWORNIK, 1961) and no systematic studies on sulfides have been made using the electron microanalyzer.

II. PHOSPHIDES AND SULFIDES

A. Phosphides

Phosphorus is usually found segregated into a mineral known as schreibersite. This mineral is a phosphide of iron, nickel, and cobalt whose stoichiometric composition corresponds to the formula $(Fe–Ni–Co)_3P$. In general the composition of the mineral fluctuates between the following limits; iron from 50 to 70 wt.%, nickel from 35 to 16 wt.%, phosphorus from 15·5 to 16 wt%. and cobalt less than 1 wt.%. Another form of phosphide with the same stoichiometric composition, called rhabdite, is also very abundant. It exists as minute inclusions, observed in cross section in the form of squares or rhombi, scattered through the main mass of a meteorite.

The formation of schreibersite has been discussed by only a few investigators (HENDERSON and PERRY, 1958; Vogel, 1958). It has been suggested (HENDERSON and PERRY, 1958) that the phosphide existed as essentially an iron phosphide(Fe_3P) at high temperatures. That is, they suggest that after the iron-nickel alloy has solidified, the phosphide which is still in the liquid state, contains much less than 15 wt.% Ni. As the metallic meteorite continues to cool, the phosphide solidifies. After solidification, nickel from the γ phase diffuses into the phosphide replacing the iron which in turn migrates to the zone surrounding the phosphide. This nickel poor zone would be in the γ phase at high temperatures and would transform to α (swathing kamacite) at lower temperatures.

The ternary phase diagram of Fe–Ni–P (Vogel and BAUR, 1931) can be used as a guide in order to explain the formation of schreibersite and rhabdite in meteorites. The two incongruently melting compounds Fe_3P and Ni_3P have complete solid solubility in one another which explains how it is possible to have a varying Ni content in $(Fe–Ni)_3P$.

It was shown (VOGEL, 1958) that in alloys having the same Fe, Ni, and P contents as found in hexahedrites, rhabdite needles are precipitated from solid solution below 500°C. Therefore rhabdite must have formed by a precipitation reaction and not from the molten state. Two possible methods for the formation of schreibersite were suggested by VOGEL, cooling from the melt and solid state precipitation. Several meteorite samples were heated above the eutectic temperature (1050°C) then cooled rapidly (VOGEL, 1958). The resulting eutectic structure of the schreibersite is quite similar to the structure of phosphides found in the reheated zones of meteorites. Meteorite samples were also heated to temperatures below the eutectic (900 to 700°C) and the schreibersite precipitates completely dissolved. This indicates that schreibersite probably formed by precipitation in the parent body of the meteorite. The formation of the swathing kamacite zone around the phosphide was not discussed.

It will be shown that both rhabdite and schreibersite form by precipitation in

the solid state and that the size and composition of the resulting phosphides is dependent on the nucleating temperature and the time available for the growth of these precipitates. It should also be noted that massive phosphides which show no apparent relation to the Widmanstätten pattern in octahedrites, must form directly from the liquid state.

B. Sulfides

Sulfur is found segregated into a mineral called troilite, a monosulfide of iron, its stoichiometric composition corresponding to the formula FeS. The inclusions are usually in irregular rounded forms and can reach large dimensions. Very often troilite is enclosed by a layer of schreibersite or by a region of swathing kamacite. Occasionally troilite is observed as scattered plates of lamellae with a definite cubic orientation unrelated to the octahedral pattern. These particles are called Reichenbach lamellae.

It was suggested (HENDERSON and PERRY, 1958) that molten FeS is immiscible in liquid Fe–Ni and that it would segregate from the metallic Fe–Ni as the meteorite solidifies. At a temperature of about 1000°C, the liquid FeS solidifies and forms a troilite precipitate which has no orientation relationship to the Fe–Ni matrix.

Another investigator (Vogel, 1958) also believes that troilite forms from the liquid state. The Fe–Ni solid solution forms first as the meteorite cooled from the liquid state and the remaining liquid forms a eutectic structure at about 975°C which is surrounded by solid solution Fe–Ni. The sulfide homogenizes upon cooling and assumes the rounded forms usually seen in the final structure.

As will be shown later, troilite forms not only from the melt but also by solid state precipitation. These precipitates form at a temperature above the nucleation temperature of the phosphides. As the temperature decreases, these precipitates grow because of the decreasing solubility of sulfur in the kamacite phase.

III. EXPERIMENTAL

A. Electron microanalyzer

The details and construction of various electron microanalyzers are readily available in the literature (CASTAING, 1952; WITTRY, 1957; BIRKS and BROOKS, 1957; MACRES, 1958; MULVEY, 1959; PETERSON, 1961), and will not be discussed here. The Fe, Ni, and Co radiation was measured by a North American Phillips proportional counter using a bent LiF crystal and the P and S radiation was analyzed using a bent mica crystal and a North American Phillips flow proportional counter. A helium path from exit port to counter was used to reduce the absorption of the soft X-rays.

B. Specimens and specimen preparation

Three meteorites were used in the investigation; the Grant, Canyon Diablo, and Breece. The compositions of these meteorites are given in Table 1. Each meteorite was mounted in a one-inch bakelite mount along with small pieces of pure Co, Fe and Ni which were used as standards. The sulfur standard was a sulfide of stoichiometric FeS_2 (pyrite) and the phosphorus standard was a hard brittle phosphide of stoichiometric MnP.

Table 1. Compositions of the Grant, Canyon Diablo and Breece meteorites

Meteorite	Type	wt.% Fe	wt.% Ni	wt.% Co	wt.% P	wt.% S	Reference
Grant	Med. octahedrite	88·63	9·35	0·63	0·57	0·03	HENDERSON (1941)
Canyon Diablo	coarse octahedrite	89·17	7·33	0·51	0·26	0·01	MERRIL (1913)
		—	7·15	0·50	—	—	GOLDBERG *et al.* (1951)
Breece	Med. octahedrite	89·63	9·17	0·64	0·57	trace	HENDERSON and PERRY (1958)

It has been shown in this laboratory that correct surface preparation is extremely important in obtaining reliable data from the electron probe. Therefore the meteorite specimens and standards were carefully polished down through $\frac{1}{4}\mu$ diamond paste and the usual etching procedure was eliminated. The samples were examined under the microscope and certain areas were picked for analysis. These areas were taken marked by microhardness indentations so that they could be readily identified in the light optics of the electron probe.

C. Determination of chemical compositions

The intensity ratio I_A/I_A^0, where I_A^0 is the intensity from the pure element A, is not directly proportional to the composition C_A. The intensity ratio must be corrected for X-ray absorption and X-ray fluorescence because of the other elements present in the specimen. For binary systems a correction curve can be determined by using standard alloys. In some cases, this may not be practical, especially when working with ternary systems. For these situations calculations can be made which correct for X-ray absorption and fluorescence (CASTAING, 1952; CASTAING and DESCAMPS, 1955).

The ratio of measured intensity of radiation from element A in an alloy containing i elements is given by:

$$I_A/I_A^0 = \frac{C_A f_A(\chi)}{f_A^0(\chi)}\left[1 + \sum_i \frac{I_A'}{I_A}\right]$$

where the fluorescence term must be summed for all elements in the alloy which fluoresce element A. The above terms have their usual meanings as given in the literature (CASTAING, 1960).

The correction curve for Fe–S was calculated and checked by two standard alloys. Fig. 1 shows the correction curves for the ternary Fe–Ni–P. The Fe, Ni and P intensities are measured with the electron microanalyzer and any two intensity ratios are sufficient to determine the composition of a given area. However, the composition was determined by the intersection of the three intensity ratios. A correlation of $\pm\frac{1}{2}$ weight per cent is the accuracy that was obtained.

IV. RESULTS

Electron microanalyses of numerous phosphide and sulfide precipitates were made. Many of the phosphides had so many cracks in them that accurate X-ray intensities could not be measured. Fig. 2 shows the position of an electron probe

trace across a phosphide in the Breece meteorite 100 μ in width. Fig. 3 gives the results of the scans of Co, Fe and Ni across the area. The large fluctuations in intensity within the phases are due to the presence of cracks within the phosphide. The composition of the precipitate as determined from the correction curves are 34·8 wt.% Ni, 49·5 wt.% Fe, 15·6 wt.% P and 0·1 wt.% Co. This gives a molar composition of 29·9 at.% Ni, 44·8 at.% Fe and 25·3 at.% P, which is almost exactly the stoichiometric composition of $(Fe–Ni–Co)_3P$. The swathing kamacite is 20 to 30 μ

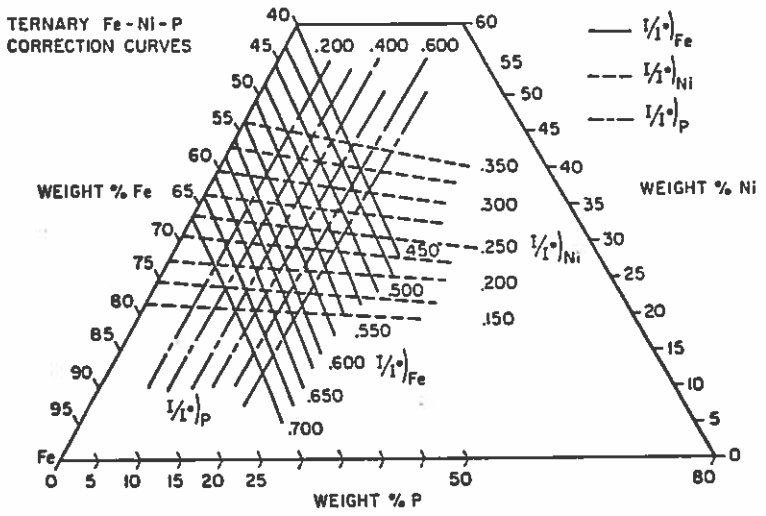

Fig. 1. Ternary Fe–Ni–P correction curves.

in width and shows a depletion of nickel from 7·0 wt.% in matrix kamacite to 6·3 wt.% at the phosphide-kamacite boundary.

A phosphide about 85 μ in width gave scans with large variances in the X-ray intensity due to the presence of cracks. However, a steady intensity was obtained in non-cracked areas and the composition of the phosphide is 36·7 wt.% Ni, 48·0 wt.% Fe, 15·2 wt.% P, and 0·1 wt.% Co. The molar composition is 31·6 at.% Ni, 43·5 at.% Fe, 24·9 at.% P, which is again in good agreement with the composition of $(Fe–Ni–Co)_3P$. The region of swathing kamacite was 30 μ wide and shows a decrease in Ni content fron 7·0 to 6·0 wt.%.

In the Grant meteorite, a large phosphide band was studied (Fig. 4). It is 500 μ wide and has a swathing kamacite border 40 μ in width. The nickel content exhibits a gradient in the border from 6·9 wt.% in the matix kamacite to 6·0 wt.% at the kamacite-phosphide interface. On the basis of the correction curves, the composition of the band is 23·4 wt.% Ni, 61·2 wt.% Fe, 15·3 wt.% P and 0·15 wt.% Co (19·8 at.% Ni, 55·4 at.% Fe, and 24·8 at.% P). The Fe, Ni, Co and P intensities were constant across the phosphide.

Figure 5 shows a large troilite precipitate (160 μ) in the Grant meteorite which was scanned with the electron probe. The troilite was in part surrounded by a phosphide 70 μ wide. The Ni, Fe and S traces taken across this area are shown in

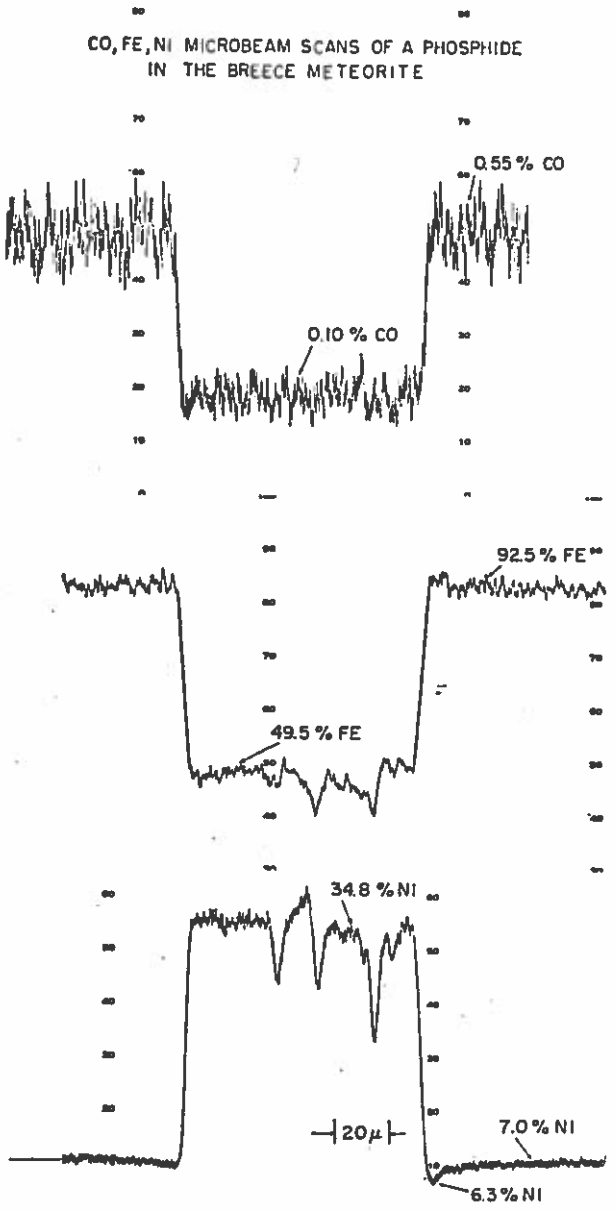

Fig. 3. Co, Fe, Ni microbeam scans of a phosphide in the Breece meteorite.

Fig. 6. There is no sulfur present in the phosphide and the sulfide contains no nickel.

The phosphide has a gradient of Ni and Fe within it. The Ni is highest at the troilite-phosphide interface and lowest at the phosphide-kamacite interface. The Fe gradient is exactly opposite, having the highest amount of Fe at the phosphide-kamacite interface. The phosphorus content is constant across the phosphide and the sulfur and iron content is constant across the sulfide. At the kamacite-phosphide border, the composition of schreibersite is 36·3 wt.% Ni, 48·3 wt.% Fe, and 15·4 wt.% P (31·3 at.% Ni, 43·6 at.% Fe, 25·1 at.% P), and at the phosphide-troilite border the composition is 38·1 wt.% Ni, 46·5 wt.% Fe and 15·4 wt.% P (32·8 at.% Ni, 42·1 at.% Fe, 25·1 at.% P). The precipitate is identified as $(Fe–Ni)_3P$ with variable amounts of Fe and Ni.

Using correction curves for the binary system Fe–S, the Fe and S intensity data give the composition of troilite as stoichiometric FeS. Swathing kamacite is present on both sides of the scan. There is a decrease in the Ni content of 1·4 wt.% in the zone on the phosphide side and 1·9 wt.% on the sulfide side of the scan. These gradients are 20 and 30 microns wide respectively.

Another phosphide in the Grant meteorite shows a gradient of Fe and Ni across its 75 μ width. At the high Ni end the composition is 37·5 wt.% Ni, 47·4 wt.% Fe 15·0 wt.% P (33·0 at.% Ni, 42·0 at.% Fe, 25·0 at.% P). At the low Ni end the composition was found to be 34·3 wt.% Ni, 50·7 wt.% Fe and 15·0 wt.% P (29·0 at.% Ni, 46·0 at.% Fe 25·0 at.% P). The Co content is 0·05 wt.%. The swathing kamacite is 15 μ wide and shows a Ni decrease of 1·2 wt.%.

Several rhabdite particles from the Canyon Diablo meteorite were examined. One precipitate is 15 μ in width (Fig. 7) and has a composition of 43·6 wt.% Ni, 41·2 wt.% Fe and 15·2 wt.% P (37·7 at.% Ni, 37·4 at.% Fe, 24·9 at.% P) corresponding to schreibersite. The swathing kamacite is 18 μ wide and the concentration of Ni decreased from 6·8 to 6·0 wt.% at the interface between kamacite and the phosphide.

Other precipitates which were less than 10 μ wide gave unreliable results. The composition of these phosphides indicated that they were low in phosphorus, for example, one gave 43·9 wt.% Ni, 43·2 wt.% Fe and 12·9 wt.% P. The composition determination may be inaccurate by as much as 5 weight per cent. The swathing kamacite in this case was 10 μ wide and the Ni content decreased by 0·6 wt.% over the zone.

V. Discussion

The phosphides identified in the three meteorites were all of a composition $(Fe–Ni–Co)_3P$ corresponding to that of schreibersite. They contained 15·5 $\pm$ 0·5 wt.% phosphorus with variable amounts of iron and nickel. It has been claimed that meteorites contain no more than 0·75 wt.% phosphorus (Krinov, 1960) and according to the Fe–P phase diagram (Hanson, 1958), phosphorus of this amount is soluble in alpha iron at temperatures below that of the eutectic (1050°C). The influence of Ni should be to lower the solubility of phosphorus. However, phosphorus, in the amount found in iron meteorites, is still soluble in the metallic Fe–Ni below the temperature at which the liquid phase is present (Vogel, 1958). Therefore, if phosphides formed directly from the melt non-equilibrium solidification must have

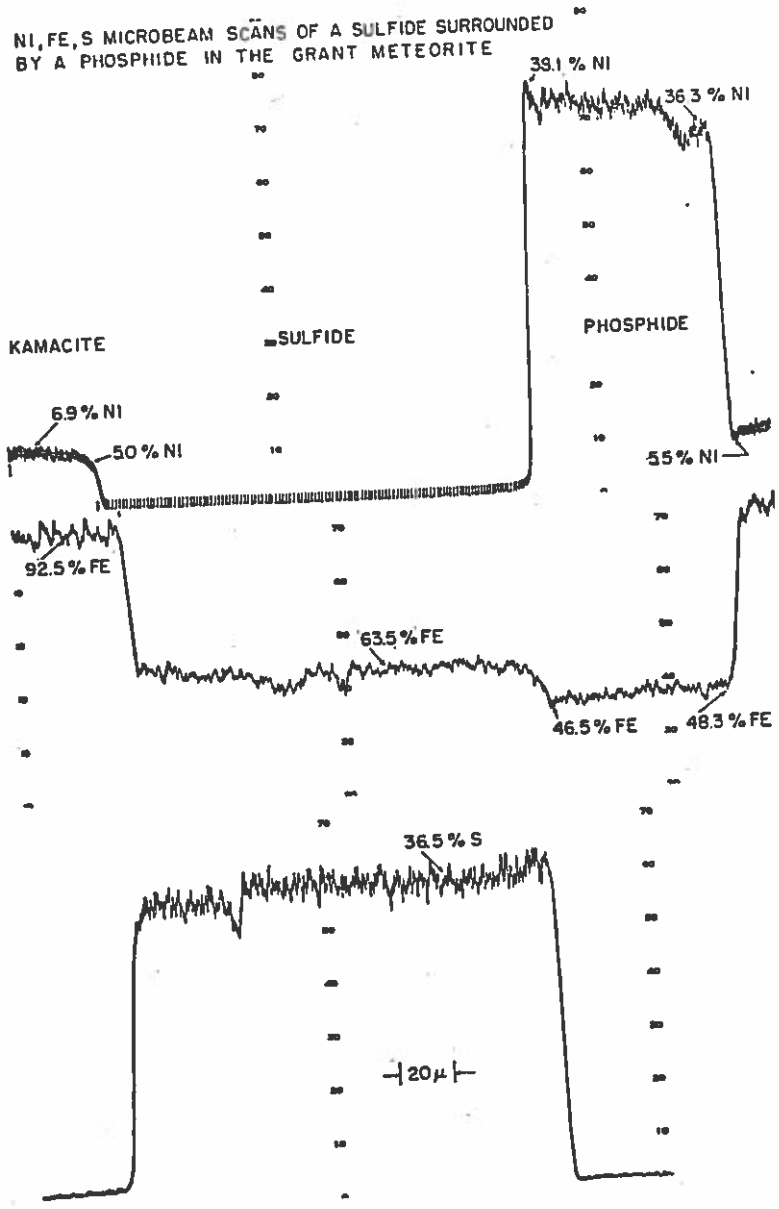

Fig. 6. Ni, Fe, S microbeam scans of a sulphide surrounded by a phosphide in the Grant meteorite.

occurred. The fact that most metallic meteorites indicate that they were single crystals in the gamma phase (Perry, 1944; Mason, 1962) and have massive phase structures, chemical equilibrium must have been maintained in most metallic meteorites at temperatures above 700°C. Since chemical equilibrium is maintained to 700°C, phosphorus cannot come out of solid solution above the eutectic temperature. The formation of schreibersite by non-equilibrium cooling is therefore highly improbable. Therefore there is only one possible mechanism for the formation of the phosphides observed in the kamacite phase; that is, solid state precipitation.

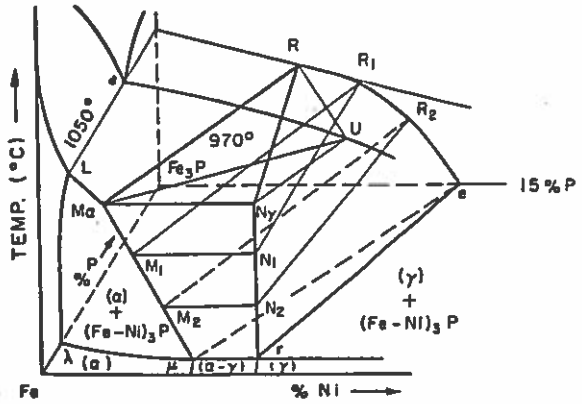

Fig. 8. Fe rich corner of Fe–Ni–P phase diagram.

Phosphides that have eutectic structures were most likely formed by the reheating of the meteorite above the eutectic temperature followed by rapid cooling.

The formation of schreibersite and rhabdite from the solid state can be explained by means of the iron corner of the Fe–Ni–P system. This phase diagram is shown schematically in Fig. 8. U is the composition of the melt at the lowest temperature (970°C) at which it is still in equilibrium with α. At this temperature and at 1 atm pressure there is a non-variant reaction M_α + melt $U \rightleftharpoons N_\gamma + R$, where R is the composition of $(Fe–Ni)_3P$ that forms at this temperature. The compositions at the phase boundaries are not given on the diagram because they are not known to any degree of accuracy. However, the general shape of the ternary diagram (Vogel 1931) is useful in describing the formation of the phosphides.

Hexahedrites have a single phase structure of kamacite (α). When this type of meteorite cools its composition is such that it will pass through the saturation face $\lambda\mu M_\alpha L$ of the α phase and enter the two phase region α + $(Fe–Ni)_3P$, causing the precipitation of phosphides. The temperature at which these precipitates form is determined by the amount of Ni and P in solid solution. When the temperature at which precipitation begins is low, the particles that form are called rhabdites.

In octahedrites, as the temperature of the meteorite decreases, α phase precipitates from γ as it cools below the $(\alpha + \gamma)/\gamma$ surface in the Fe–Ni–P phase diagram. It has been found by electron probe measurements that kamacite has a greater

solubility for phosphorus than taenite. The Grant meteorite has a P content of 0·07 ± 0·01 wt.% in kamacite and 0·025 ± 0·01 wt.% in taenite while the Breece meteorite has a P concentration of 0·075 ± 0·01 wt.% in kamacite and 0·015 ± 0·01 wt.% in taenite. The redistribution of P from γ to α probably occurs even at low temperatures because of the relatively high diffusivity of phosphorus.

As the kamacite grows at the expense of taenite, it also must enrich in nickel. Nickel diffuses from the taenite-kamacite interface into the kamacite and at low temperatures a nickel gradient will be present in the kamacite with a minimum in the center of the band. Therefore it is expected that the center of the kamacite phase will have a lower concentration of nickel than the equilibrium value.

Therefore, upon further cooling the phosphorus content in the nickel poor region of the kamacite exceeds the saturation face $\lambda\mu M_a L$ of the α solid solution and enters the two phase region $\alpha + (Fe\text{–}Ni)_3P$ where schreibersite precipitates. To the best of our knowledge, schreibersite, which is less than 1000 μ in width is always found within the kamacite phase which is in accordance with this theory. Therefore the precipitation of these phosphides cannot begin before the Widmanstätten pattern forms. This process is illustrated in Fig. 9 which shows the Widmanstätten pattern of the Carlton meteorite. After the nucleation of the Widmanstätten platelets, the phosphide particles begin to precipitate and are therefore found in the centers of the fully formed kamacite plates.

According to the Fe–P phase diagram, the solubility of phosphorus in pure iron is 1·0 wt.% at 735°C, 0·25 wt.% at 500°C and 0·015 wt.% at room temperature. The phosphorus content of the Breece and Grant meteorites is 0·57 wt,% and that of the Canyon Diablo meteorite is 0·26 wt.%. Therefore if one assumes that no undercooling occurs before nucleation, phosphide precipitation in the form of schreibersite begins around 650°C in the Grant and Breece and the precipitation of rhabdite at about 500°C in the Canyon Diablo. The effect of Ni is to decrease the solubility of phosphorus in the matrix which will increase the temperature of nucleation slightly.

It can be seen from the Fe–Ni–P phase diagram (Fig. 8) that a phosphide which lies on the same tie-line with a particular composition of kamacite in the $\alpha + (Fe\text{–}Ni)_3P$ two phase field, increases in nickel with decreasing temperature. However, if equilibrium conditions prevail at low temperatures, all the phosphides must have the same compositions no matter what their nucleation temperature was. This condition is not satisfied in meteoric phosphides. It appears that the smaller the size of the precipitates, the higher is the Ni content found in the particles. The data supporting this trend is given in the following table. This data indicates that the largest phosphides have the lowest Ni contents and the rhabdite precipitates have the highest Ni contents. This trend was also found by HENDERSON and PERRY (1958) from examinations of phosphides by chemical analysis. Since the phosphides do not have the equilibrium compositions given by the ternary diagram, a non-equilibrium growth process must have taken place.

After the nucleation of a phosphide particle, the process of growth begins. Evidence that this process occurred is given by the presence of the swathing kamacite region surrounding every phosphide. This is the area through which nickel and phosphorus diffuse from the matrix kamacite to the growing phosphide.

For the phosphides to grow, both phosphorus and nickel must diffuse from

Table 2. Phosphides in the Grant, Breece, and Canyon Diablo Meteorites

Meteorite	Phosphide	Width (μ)	% Ni (average)	% Ni Depletion at Interface	Width of Swathing Kamacite (μ)
Grant (Fig. 4)	Schreibersite	500	23·4	0·9	40
Breece (Fig. 2)	Schreibersite	100	34·8	0·7	25
Breece	Schreibersite	85	36·7	1·0	30
Grant	Schreibersite	75	35·9	1·2	15
Grant (Fig. 5)	Schreibersite	70	37·2	1·4	20
Canyon Diablo (Fig. 7)	Rhabdite	15	43·6	0·8	18
Canyon Diablo	Rhabdite	10	43·9	0·6	10

kamacite into the precipitate. The diffusion coefficient of P in steel is: $D(P, \text{Steel}) = (4{\cdot}5 \times 10^{-2}) \exp(-43{,}000/RT)$ (BARRER, 1951) and the diffusion coefficient of Ni in kamacite is $D(\text{Ni}, \alpha) = 1{\cdot}4 \exp(-58{,}7000/RT)$ (HIRANO *et al.* 1961). The diffusion of phosphorus to the phosphide is much faster than that of Ni. Therefore the diffusion of nickel to the phosphide controls its rate of growth.

With certain simplifying assumptions, one can calculate the growth rate of the phosphides and from this information the probable nucleation temperature and precipitate size. Since the phosphides precipitate below the temperature at which the Widmanstätten pattern begins to form, the phosphides then formed within the approximate temperature range from 750 to 350°C. Within this range the cooling curve for meteoric bodies may be assumed to be linear.

By using Fick's second law and by applying the appropriate boundary conditions for the growth of a planar interface, the phosphide growth distance as a function of time and temperature can be calculated (JOST, 1960). The composition of the kamacite may be expressed by the following equation:

$$C_\alpha = A_\alpha + B_\alpha \operatorname{erf}\left(\frac{x}{2\sqrt{D_\alpha t}}\right) \tag{1}$$

where D_α is the interdiffusion coefficient in the α phase. The movement of the interface (ξ) is a function of time (t) and follows a parabolic law:

$$\xi = 2\gamma\sqrt{D_\alpha t} \tag{2}$$

Figure 10 shows the variation of Ni content as the phosphide grows. The Ni content in kamacite before precipitation is C_α' and the Ni contents at the phosphide-kamacite interface are C' and C''. The initial and boundary conditions are:

at $t = 0, \quad x > 0, \quad C_\alpha = C_\alpha'$

$t > 0, \quad x = \xi, \quad C_\alpha = C'$ (3)

Solving equation (1) using the above conditions (2) and (3)

$$C_\alpha = \frac{C' - C'_\alpha \operatorname{erf}(\gamma)}{1 - \operatorname{erf}(\gamma)} + \frac{C'_\alpha - C'}{1 - \operatorname{erf}(\gamma)} \left(\operatorname{erf} \frac{x}{2\sqrt{D_\alpha t}} \right) \tag{4}$$

γ may be evaluated from a mass balance:

$$(C'' - C') \frac{d\xi}{dt} = D_\alpha \left(\frac{\partial C}{\partial X} \right)_{X>\xi} \tag{5}$$

Differentiating equations (2) and (4) and substituting into equation (5), one obtains the following relation:

$$\sqrt{\pi}\gamma e^{\gamma^2}(1 - \operatorname{erf}(\gamma)) = \frac{C'_\alpha - C'}{C'' - C'} \tag{6}$$

Figure 10 gives a plot of the constant γ versus $(C'_\alpha - C')/(C'' - C')$. Using equation (2) and evaluating γ from Fig. 10, one can calculate the width of the phosphide (2ξ) for any given temperature and time.

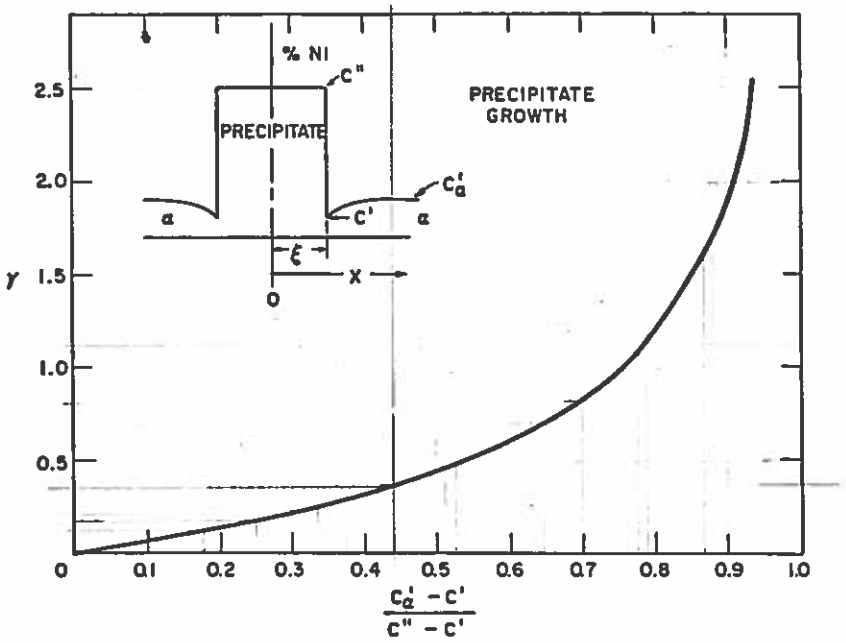

Fig. 10. Schematic of precipitate growth and curve of γ versus the parameter, $C_\alpha' - C'/C'' - C'$.

The conversion from a linear cooling rate S, starting at a given temperature T_0, into an equivalent time at T_0 can be calculated (ARMSTRONG, 1958). The total effect is the same as if the diffusion were carried out at the initial nucleating temperature. The equivalent time is given by:

$$t_{\text{equiv.}} = \frac{RT_0^2}{SQ} \tag{7}$$

where Q is the activation energy for diffusion.

The following table gives the values of the widths of the phosphides (2ξ) for different nucleating temperatures and cooling rates.

Table 3. Phosphide widths

Nucleating Temp.			Time to cool from 750°C to 350°C					
			10^8 years		10^7 years		10^6 years	
T_0(°C)	2γ	D_α (cm²/sec)	t_{equiv} (sec)	2ξ (μ)	t_{equiv} (sec)	2ξ (μ)	t_{equiv} (sec)	2ξ (μ)
700	0·0208	$1·0 \times 10^{-13}$	$2·53 \times 10^{14}$	2116	$2·53 \times 10^{13}$	670	$2·53 \times 10^{12}$	212
650	0·0244	$0·2 \times 10^{-13}$	$2·29 \times 10^{14}$	1052	$2·29 \times 10^{13}$	332	$2·29 \times 10^{12}$	106
600	0·0228	$0·3 \times 10^{-14}$	$2·04 \times 10^{13}$	356	$2·04 \times 10^{13}$	116	$2·04 \times 10^{12}$	36
550	0·0248	$0·4 \times 10^{-15}$	$1·82 \times 10^{14}$	134	$1·82 \times 10^{13}$	42	$1·82 \times 10^{12}$	13
500	0·0266	$0·5 \times 10^{-16}$	$1·60 \times 10^{14}$	48	$1·60 \times 10^{13}$	15	$1·60 \times 10^{12}$	4·8
450	0·0312	$0·4 \times 10^{-17}$	$1·40 \times 10^{14}$	14	$1·40 \times 10^{13}$	4·4	$1·40 \times 10^{12}$	1·4
400	0·0312	$0·15 \times 10^{-18}$	$1·21 \times 10^{14}$	2·6	$1·21 \times 10^{13}$	0·8	$1·21 \times 10^{12}$	0·2
350	0·0350	$0·5 \times 10^{-20}$	$1·03 \times 10^{14}$	0·6	$1·03 \times 10^{13}$	0·2	$1·03 \times 10^{12}$	0·06

The above table shows that schreibersite precipitates the size of those in Fig. 4 (500 μ) must have nucleated between 650 and 700°C in order to grow to such a size. The phosphides of a size about 100 μ in width precipitated between 550 and 600°C and the rhabdite particles nucleated between 450 and 500°C. These nucleation temperatures are in agreement with the values given by VOGEL and the binary phase diagrams as discussed before. The time that it takes to cool between 750 and 350°C fall in the range between 10^7 and 10^8 years. These times are in agreement with estimates (MASSALSKI and PARK, 1961) for the total time taken for the formation of the Widmanstätten pattern (under conditions of equilibrium and without large pressures), which may be taken to be approximately 10^7 years for a 200 km radius metallic body and 10^8 years for a 200 km radius silicate body having a small metallic core.

The non equilibrium composition of the phosphides is due to the reduced flux of Ni into the precipitate at temperatures below T_0. The composition gradient, $(\partial C/\partial X)_{X>\xi}$ is decreased greatly as the temperature decreases, and at a lower temperature is inadequate to maintain the growth of the phosphide. Since the phosphide can no longer grow, it retains the high temperature Ni concentration throughout the rest of the cooling period. The phosphide probably stops growing about 50 to 100° below T_0. In this temperature range most of the phosphide growth occurs which can be seen from Table 3. Since the Ni content of the phosphide increases with decreasing nucleation temperatures, the rhabdite particles which nucleated below 500°C have the highest Ni contents and the schreibersite particles which nucleated at more than 650°C have the lowest Ni contents. Since the rhabdite particles nucleated at the lowest temperatures, they have the shortest time to grow and therefore the smallest size.

In several meteorites massive schreibersite particles, which have a width greater than 100 μ, have been found. The phosphorus content of meteorites containing such particles is probably grossly underestimated. This is because most of the phosphorus is segregated in the massive phosphides, which makes it difficult to

obtain an accurate average phosphorus content for the meteorite. The solubility limit of phosphorus in the solid state will be exceeded at high temperatures and the phosphide will nucleate in the taenite phase or possibly the phosphide may form directly from the melt. Even in meteorites where massive schreibersite forms, the phosphorus solubility limit continues to decrease as cooling proceeds and at lower temperatures other phosphides will precipitate in the kamacite phases of the Widmanstätten pattern as described above.

The binary phase diagrams, Fe–S and Ni–S show a sulfur solubility in δ iron of 0·18 wt.%, but a solubility of only 0·005 wt.% in nickel (METALS HANDBOOK, 1948). Since the δ phase does not form when the Ni content is over 4·5 wt.%, sulfur has very limited solubility in meteorites. As the meteorite cools sulfur in excess of the solubility limit remains in the liquid state until the eutectic temperature at about 985°C. As this temperature a eutectic structure of FeS and γ(Fe, Ni) forms which is in equilibrium with γ(Fe–Ni). Nickel is soluble in the liquid phase, but not in eutectic FeS. The very large sulfide particles found in meteorites are formed in this manner which is in agreement with previous studies (HENDERSON and PERRY, 1958; VOGEL, 1958).

The solubility of sulfur in γ(Fe, Ni) decreases as the meteorite cools below the eutectic temperature. Sulfides are then precipitated in the solid state from the supersaturated γ phase and at lower temperatures from the α phase. The sulfur solubility in the Grant and Breece meteorites as measured with the electron probe is 0·02 wt.% in kamacite and 0·005 wt.% in taenite. Examples of sulfides which form is the solid state are the Reichenbach lamellae and troilite particles which are of the same general sizes as the phosphides.

The diffusion of sulfur in Fe is much faster than the diffusion of Fe in kamacite; $D(S, \mathrm{Fe}) = (4{\cdot}8 \times 10^{-6}) \exp(-23{,}400/RT)$ (BARRER, 1951) versus $D(\mathrm{Fe},\alpha) = 2{\cdot}0 \exp(-60{,}000/RT)$ (BUFFINGTON *et al.* 1961). Therefore the growth of the precipitate in the solid state is controlled by the diffusion of Fe from the sulfide. Both Fe and Ni are rejected from the growing sulfide and since a larger amount of Fe is rejected from the volume occupied by the troilite particle, a build up of Fe in the kamacite immediately surrounding the interface between kamacite and troilite occurs. The area would then contain a depleted zone of nickel. The sulfide shown in Fig. 5 probably nucleated at about 700°C and grew almost to its full size before the phosphide nucleated at its boundaries at about 550°C.

VI. CONCLUSIONS

It is apparent that schreibersite and rhabdite found in kamacite formed by solid state precipitation. At about 100°C below their nucleation temperature, the phosphides stop growing due to the large depletion of Ni in the region surrounding the precipitate and they retain their high temperature composition during further cooling. The time necessary for the growth of the phosphides is also in agreement with the calculations of MASSALSKI and PARK (1961) for the time of formation of the Widmanstätten patterns in octahedrites. The massive sulfides formed directly from the melt. However, troilite inclusions of smaller sizes formed by solid state precipitation and grew by forming an iron rich region (swathing kamacite) around the sulfide.

Fig. 2. Photomicrograph of a phosphide area in the Breece meteorite. 250 ×. No etchant

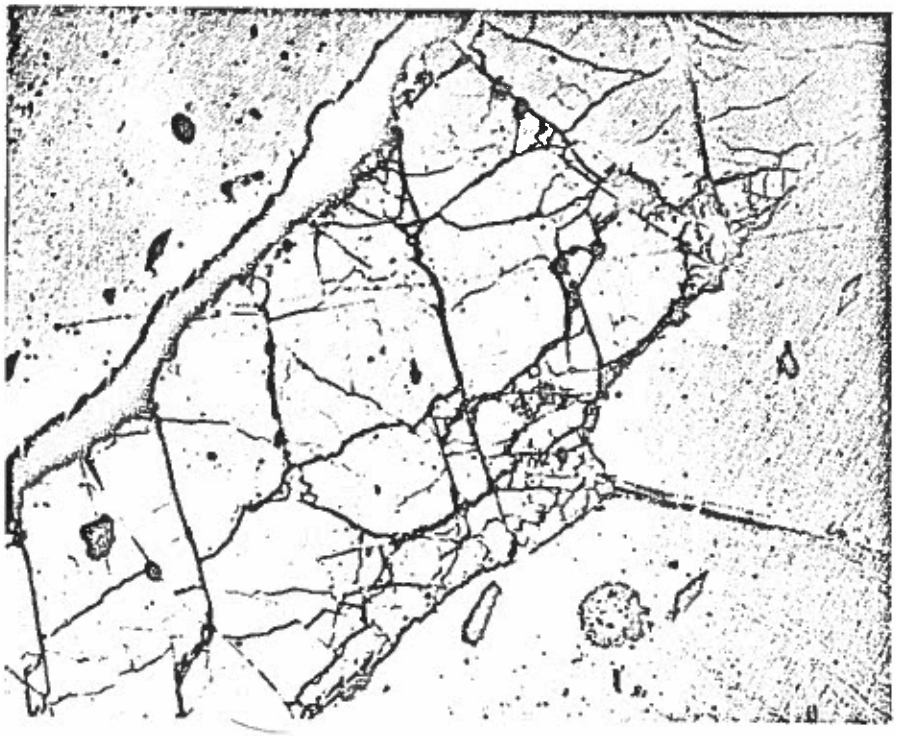

Fig. 4. Photomicrograph of a phosphide area in the Grant meteorite, 100 ×. No etchant.

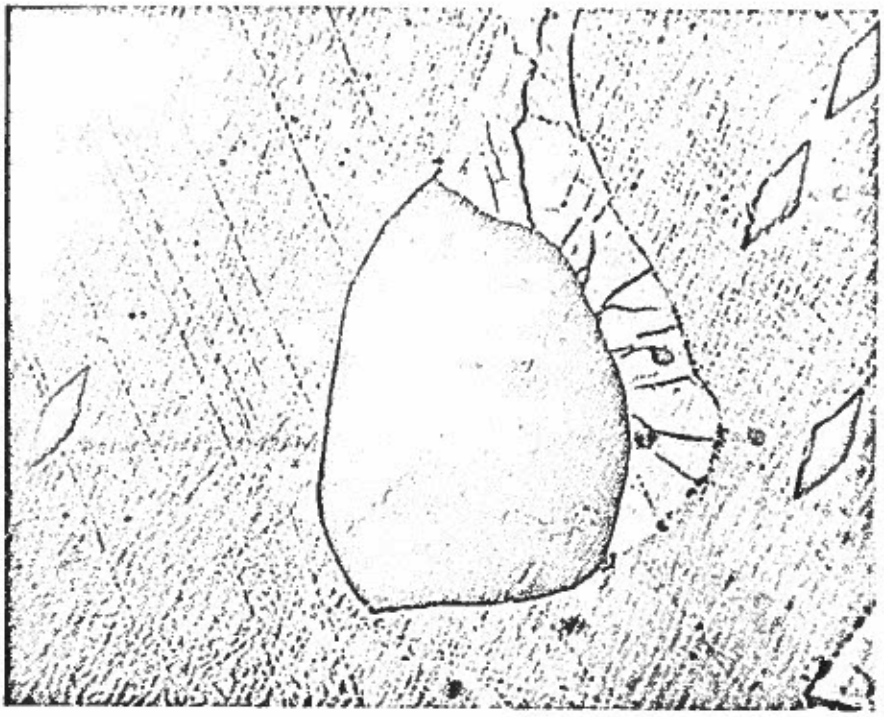

Fig. 5. Photomicrograph of a sulfide area surrounded by a phosphide band in the Grant meteorite. 250 ×. No etchant.

Fig. 7. Photomicrograph of rhabdite precipitates in the Canyon Diablo meteorite, 150 ×. No etchant.

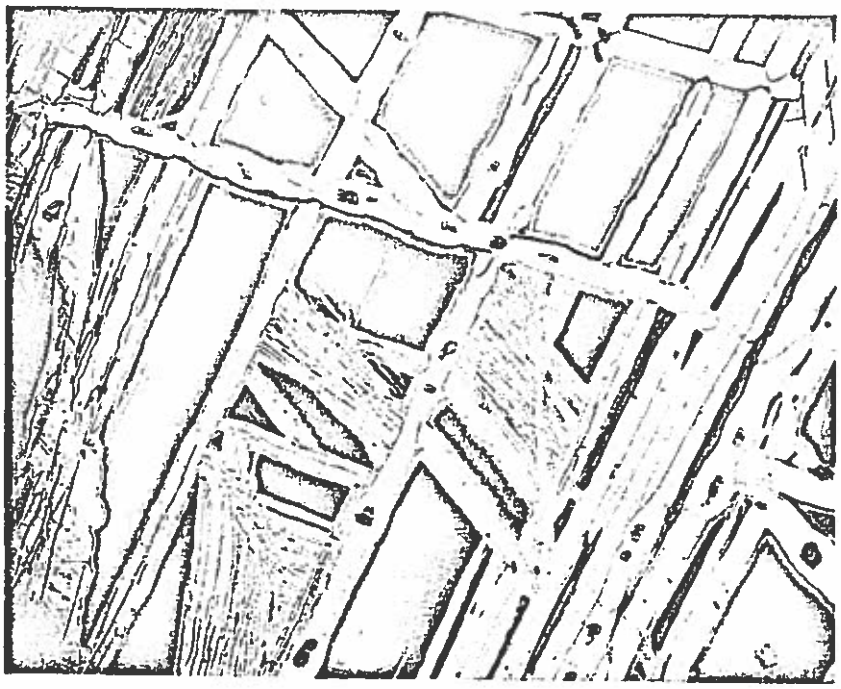

Fig. 9. Widmanstätten pattern in the Carlton meteorite, 20×.

Acknowledgements—The authors wish to thank Professor C. S. Smith, Mr. Rodney Hanneman, Mr. Dennis Brown, and Mr. Harold Brody for their valuble advice and assistance. Our thanks are also due to E. P. Henderson of the U.S. National Museum for the loan of the meteorite specimens.

References

Adler I. and Dwornik E. J. (1961) Geological Survey Research 1961, 263–265.
Armstrong H. L. (1958) *Trans. Met. Soc., A.I.M.E.* **212**, 450–451.
Metals Handbook (1948), *A.S.M.* Cleveland.
Barrer R. (1951) *Diffusion in and through Solids.* Cambridge.
Birks L. S. and Brooks E. J. (1957) *Rev. Sci. Instr.* **28**, 709–712.
Buffington F. S., Hirano K. and Cohen M. (1961) *Acta Met.* **9**, 434–439.
Castaing R. (1952) Ph.D. Thesis, University of Paris.
Castaing R. and Descamps J. (1955) *J. Phys. & Rad.* 304—317.
Castaing R. (1960) *Advances in Electronics and Electron Physics.* L. Martin, (Editor), **13**, Academic Press, New York. 317.
Feller-Kniepmeyer M. and Uhlig H. H. (1961) *Geochim. et Cosmochim. Acta* **21**, 257–265
Goldberg E., Uchiyama A. and Brown H. (1951) *Geochim. et Cosmochim. Acta* **2**, 1–25.
Hansen M. (1958) *Constitution of Binary Alloys.* McGraw-Hill, New York.
Henderson E. P. (1941) *Amer. J. Sci.*, **239**, 407.
Henderson E. P. and Perry S. H. (1958) *Proc. U.S. Nat. Mus.* **107**, 339–403.
Hirano K., Cohen M. and Averbach B. L. (1961) *Acta Met.* **9**, 440–445.
Jost W. (1960) *Diffusion in Solids, Liquids, Gases.* Academic Press, New York.
Krinov E. L. (1960) *Principles of Meteoritics.* Pergamon Press, Oxford.
Macres V. G. (1958) Sc.D. Thesis, Massachusetts Institute of Technology.
Maringer R. E., Richard N. A. and Austin A. E. (1959) *Trans. Met. Soc., A.I.M.E.*, **215**, 56–58.
Maringer R. E. and Manning G. K. (1959) *WADC Tech. Rep.* 59–164.
Mason B. (1962) *Meteorites.* John Wiley, New York.
Massalski T. B. and Park F. (1961) To be published.
Merril G. P. (1913) *Amer. J. Sci.* 4th Ser. **209**, 509–525.
Mulvey T. (1959) *Rev. Met.* **56**, 163–171.
Perry S. H. (1944) The Metallography of Meteoric Iron *U.S. Nat. Mus. Bull.* **184**, 206 pp.
Peterson N. L. (1961) Sc.D. Thesis, Massachusetts Institute of Technology.
Vogel R. (1958) *Chem. Erde*, **19**, 147–169.
Vogel R. and Baur H. (1931) *Arch. Eisenhuttenw.* **5**, 269–278.
Wittry D. B. (1957) Ph.D. Thesis, California Institute of Technology.
Yavnel A. A., Borovski I. B., Ilin N. P. and Marchukowa I. D. (1958) *Dokl. Akad. Nauk. SSSR*, **123**, 256–258.